Comparison of structural transformations and superconductivity in compressed sulfur and selenium

Sven P. Rudin
Los Alamos National Laboratory, Los Alamos, New Mexico 87545

Amy Y. Liu, J. K. Freericks, and Alexander Quandt
Department of Physics, Georgetown University, Washington, DC 20057
(Received 14 November 2000; published 21 May 2001)

Density-functional calculations are presented for high-pressure structural phases of S and Se. The structural phase diagrams, phonon spectra, electron-phonon coupling, and superconducting properties of the isovalent elements are compared. We find that with increasing pressure, Se adopts a sequence of ever more closely packed structures (β-Po, bcc, fcc), while S favors more open structures (β-Po, simple cubic, bcc). These differences are shown to be attributable to differences in the S and Se core states. All the compressed phases of S and Se considered are calculated to have weak to moderate electron-phonon coupling strengths consistent with superconducting transition temperatures in the range of 1 to 20 K. Our results compare well with experimental data on the β-Po$\rightarrow$bcc transition pressure in Se and on the superconducting transition temperature in β-Po S. Further experiments are suggested to search for the other structural phases predicted at higher pressures and to test theoretical results on the electron-phonon interaction and superconducting properties.

DOI: 10.1103/PhysRevB.63.224107 PACS number(s): 61.50.Ks, 63.20.Kr, 74.25.Kc, 74.62.Fj

I. INTRODUCTION

The chalcogens exist in a rich variety of crystal structures at ambient pressures and upon compression.[1–5] At low pressures, S, Se, and Te crystallize in different sequences of insulating twofold-coordinated molecular or polymeric structures. With enough compression, however, all three elements transform into the same body-centered orthorhombic (bco) crystal structure. The bco structure is comprised of puckered layers with each site having a coordination number of 4. With further compression, the more three-dimensional sixfold-coordinated rhombohedral β-Po structure becomes stable in all three systems. At even higher pressures, Se and Te are observed to transform from the β-Po structure to the body-centered cubic (bcc) structure, continuing the trend of increasing coordination and closer packing with pressure. It has been speculated that S should also undergo a β-Po $\rightarrow$bcc transition, but compressed phases beyond the β-Po phase have not yet been observed in S.

Electrical measurements show that S, Se, and Te are all metallic in the bco structure.[6] Further, the metallic bco phases of S, Se, and Te are observed to be superconducting with transition temperatures of approximately 10, 5, and 3 K, respectively.[7,8] Recent magnetic measurements show that the superconducting transition temperature in S jumps abruptly to 17 K upon transformation to the β-Po structural phase.[9] This is among the highest transition temperatures observed in elemental solids. Earlier calculations had predicted the hypothetical bcc phase of S to be superconducting with a similar transition temperature of about 15 K near 550 GPa.[10] As yet, no measurements of T_C have been reported on the higher-pressure phases of the heavier chalcogens.

We recently reported density-functional calculations of the structural and superconducting transitions in compressed S.[11] Our calculations predicted that unlike Se and Te, S would transform from the β-Po phase to the relatively open simple-cubic (sc) structure. The sc structure was found to be favored over a wide range of pressures, with the bcc phase eventually becoming stable at very high compressions. Further, our calculations indicated that the high superconducting transition temperature observed in the β-Po phase of S arises not from strong electron-phonon coupling, but rather from a combination of moderate coupling and a large phonon energy scale.

Here, we present a comparative study of the structural and superconducting transitions in S and Se, expanding our previous work on compressed S and presenting new results for Se. Though the two materials are chemically similar, they display striking differences in their properties under pressure. In addition to the simple-cubic structure's viability as a high-pressure phase for S but not Se, the stability of the fcc structure is another difference between the materials. An analysis of the contributions to the total energy shows that these structural differences can be understood in terms of differences between the S and Se cores. Although some of the trends in the calculated electron-phonon coupling and superconducting properties are similar in the two materials, the superconducting transition temperature is higher in S than in Se, even within the same structural phase. A comparison of the phonon spectra and electron-phonon coupling in these materials helps to explain the differences.

The remainder of this paper is organized as follows. In Sec. II, we compare and contrast the calculated high-pressure structural phase diagrams for S and Se. In Sec. III, the calculated vibrational spectra and electron-phonon coupling parameters for the high-pressure phases are presented and discussed. We also discuss ways in which our results can be tested and compared with diamond-anvil-cell-based experiments, including measurements of superconducting properties, transport coefficients, and optical conductivity. Concluding remarks are given in Sec. IV.

II. HIGH-PRESSURE STRUCTURAL PHASES

A. Method

Zero-temperature structural energetics are calculated using the plane-wave pseudopotential method within the density-functional formalism. The pseudopotentials are generated using the Troullier-Martins method.[12] Kinetic-energy cutoffs of 70 and 40 Ry are used for the plane-wave expansion of the Kohn-Sham orbitals in S and Se, respectively. For the exchange-correlation potential we use the local-density approximation as parametrized by Perdew and Zunger.[13] The nonlinearity of the exchange and correlation interaction between the core and valence charge densities is treated using a partial core.[14] The Brillouin zone for each structure is sampled on Monkhorst-Pack meshes of at least 20^3 points.[15]

Care must be taken in using pseudopotentials to describe highly compressed matter. The accuracy of the pseudopotential diminishes as the interatomic spacing becomes comparable to or smaller than the sum of the cutoff radii within which the valence wave functions are pseudized. In addition, at even smaller interatomic distances, core relaxation effects become important. The potentials used in this paper are constructed so that the all-electron and pseudo-wave functions match beyond about 1.2 and 1.7 a.u. for S and Se, respectively. As the nearest-neighbor distance is about 3.7 a.u. in bcc S at 500 GPa and about 4.4 a.u. in bcc Se at 250 GPa, we are still working within a regime where these pseudopotentials are reasonable.

B. Results and discussion

This work focuses on the β-Po and higher-pressure phases of S and Se.[16] Candidate structures investigated include bcc, sc, fcc, simple hexagonal, α-Hg, Cs-IV, and the related β-Sn structure. Only the β-Po, bcc, sc, and fcc structures were found to be competitive in energy within the pressure regime of interest. These four structures can all be described in terms of a single-atom rhombohedral unit cell with rhombohedral angles α_r of 60° (fcc), 90° (sc), approximately 104° (β-Po), and 109.47° (bcc).

Figure 1 shows the total energy for S and Se calculated as a function of the rhombohedral angle at constant unit-cell volumes. The curves for the two materials are strikingly different, leading to different sequences of high-pressure phases. In particular, for the range of volumes shown in Fig. 1, the simple-cubic structure is never competitive in energy with the other structures considered for Se, while the fcc structure is never favorable for S.

For the largest unit-cell volume shown, corresponding to roughly 80 GPa in Se, the β-Po structure with $\alpha_r \approx 104°$ is lowest in energy. At a smaller volume of 76 a.u. (roughly 140 GPa), the local minimum for β-Po Se has disappeared, and the bcc structure is favored. At even smaller volumes, the minimum at $\alpha_r = 60°$ drops below that at 109.5°, indicating a bcc to fcc transition. Comparison of the enthalpies $H = E_{\text{total}} + pV$ calculated for the different structures yields a transition pressure of 120 GPa for the β-Po→bcc transition, which is in reasonable agreement with the experimental value of 140 GPa. For the bcc→fcc transition, we predict a transition pressure of about 260 GPa.

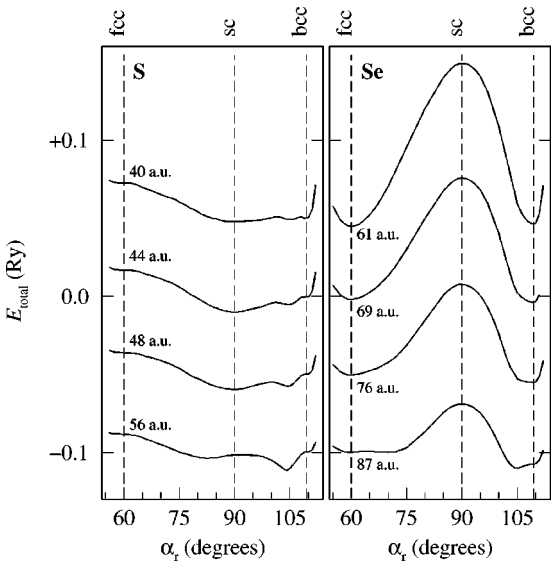

FIG. 1. Total energy vs rhombohedral angle α_r at constant volumes for S and Se. The results for S are from Ref. 11 and are reproduced here to facilitate comparison with Se. At moderate compression both elements favor the β-Po structure ($\alpha_r \approx 104°$); increased compression results in the sequence β-Po→sc→bcc for S and β-Po→bcc→fcc for Se.

As first reported in Ref. 11, S is calculated to transform from the β-Po to the sc to the bcc structure with increasing pressure. For the static lattices, we find transition pressures of 260 and 540 GPa for these structural transformations. Because of differences in average vibrational frequencies $\langle\omega\rangle$ (see Sec. III), the inclusion of zero-point energies, $E_{zp} = 3\hbar\langle\omega\rangle/2$, shifts the estimated transition pressures in S to about 280 and 500 GPa.

In terms of coordination number and packing, Se follows the expected trend of increasing coordination with pressure, going from 6 (β-Po) to 8 (bcc) to 12 (fcc). With each transformation, Se adopts a more closely packed structure. Sulfur, on the other hand, transforms from the sixfold-coordinated β-Po structure to the sc structure, which is also sixfold coordinated, but is more open. (The ratio of next-nearest to nearest-neighbor distances is 1.24 and 1.41 in the β-Po and sc structures, respectively.) While the more highly coordinated bcc structure is adopted at large compressions, the even more densely packed fcc structure is never favored. The key to the differences in the high-pressure phase diagrams of the isovalent elements lies in their cores.

Figure 2 compares the relative stability of the sc and bcc structures of S and Se as a function of volume. To facilitate the comparison, the volumes are measured with respect to the calculated equilibrium bcc volumes of $V_0^{bcc} = 98.6$ and 125.9 a.u./atom for S and Se, respectively. The total energy can be divided into the one-electron contribution, which arises from the noninteracting kinetic energy and the electron-ion interaction, the electron-electron Coulomb energy, the exchange and correlation energies, and the ion-ion energy, which includes the Ewald energy and a term that accounts for the difference between the pseudopotential and the pure Coulomb potential of the ions. In both materials, the

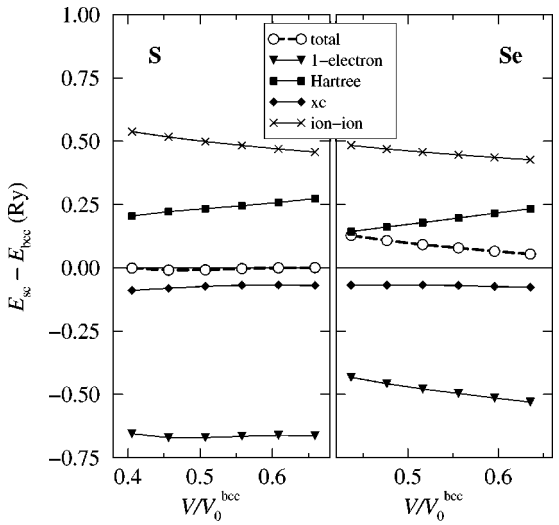

FIG. 2. Total-energy difference between the simple cubic and bcc structures as a function of volume for S and Se. Also shown are the energy differences in the one-electron, Hartree, exchange-correlation (xc), and ion-ion contributions to the total energy. Volumes are measured with respect to the theoretical zero-pressure volumes of $V_0^{bcc}=98.6$ and 125.9 a.u./atom calculated for bcc S and Se, respectively.

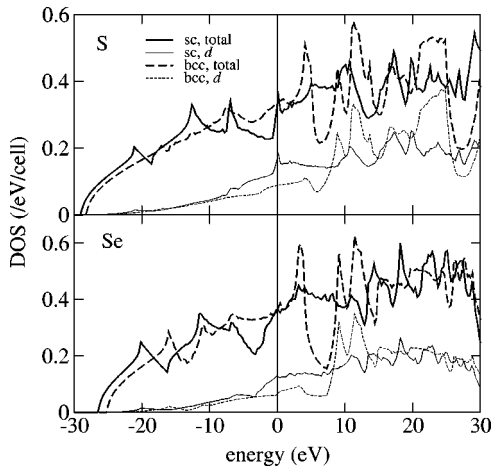

FIG. 3. Electronic density-of-states of bcc and sc S and Se. Results for S correspond to a volume of 50 a.u./atom; those for Se correspond to a volume of 70 a.u./atom. The Fermi level is at 0 eV. The *d*-projected density-of-states, plotted in lighter lines, shows that the sc structure has broader *d* bands and a higher occupation of *d* states.

repulsive Hartree and ion-ion terms favor the more closely packed bcc structure, which has a more uniform distribution of both ionic and electronic charge. The attractive electron-ion Coulomb interaction favors the more open sc structure, which tends to have very nonuniform charge distributions. The difference in total energy between the two structures is smaller than differences in the individual contributions to the total energy. Figure 2 shows that the one-electron contribution in S favors the sc structure significantly more strongly than it does in Se, thereby tipping the balance to stabilize the open sc structure. Further decomposition of the one-electron contribution shows that the kinetic energy favors the more uniform bcc structure. It is thus the electron-ion interaction that stabilizes the sc S phase.

The importance of the electron-ion interaction in producing different stable structures in S and Se can be understood in terms of the difference in their cores. In particular, since the Ne core of S contains only *s* and *p* electrons, the 3*d* states in S have no orthogonality constraint with the core, resulting in a strongly attractive *d* pseudopotential in the core region. On the other hand, in Se, which has *d* states in the core, the repulsive Pauli component of the pseudopotential largely cancels the attractive Coulomb component in the core region, resulting in a relatively weak *d* potential.

Under ambient conditions, the valence *d* states are unoccupied in both S and Se, but with compression, the *d* bands broaden and eventually cross the Fermi level. The electronic density-of-states for bcc and sc S are shown in the top panel of Fig. 3. The volume of 50 a.u./atom corresponds to about 250 GPa, which is close to the pressure at which the sc phase is calculated to become stable. The thin lines show the *d*-projected density-of-states. Since the *d* bandwidth varies roughly as C/d_{nn}^5, where C is the coordination number and d_{nn} is the nearest-neighbor distance,[17] the shorter bonds in the sc structure more than compensate for the lower coordination, leading to broader *d* bands in the sc phase as compared to the bcc phase. With more *s*-*d* transfer of electrons in the sc phase than in the bcc (or fcc) structures, the deep S *d* pseudopotential becomes important in the energetics, stabilizing the sc phase. In Se, the sc phase similarly has larger *d* occupation than the fcc and bcc phases, as shown in the bottom panel of Fig. 3. However, because the Se *d* potential is weak, this *s*-*d* transfer does not lower the one-electron energy enough to stabilize the sc structure.

Similar reasoning helps explain the absence of the close-packed fcc structure in high-pressure S. Figure 4 compares the relative stability of the fcc and bcc phases of S and Se as a function of volume. Again the different structural preferences of S and Se can be attributed to differences in the one-electron contributions to the total energy. With increasing compression, the one-electron energy in S increasingly favors the bcc structure, while in Se it increasingly favors the fcc structure. In both materials, the kinetic energy favors the more uniformly distributed fcc structure while the electron-ion term favors the bcc structure. With the deeper *d* pseudopotential in S, the importance of the electron-ion term in S is enhanced, stabilizing the bcc structure. The difference in openness between the fcc and bcc structures is of course much smaller than that between the sc and bcc structures, so in comparisons of the fcc and bcc structures, the energy differences are smaller and the energy balance is more subtle.

This discussion of the differences between S and Se and the important role of the presence of *d* states in the core suggests that the heavier chalcogen Te should be similar to Se in terms of high-pressure structural phases. Indeed, like Se, Te is observed to transform from the β-Po structure to the bcc structure with pressure.[5] In our calculations, as well as earlier ones by Kirchhoff *et al.*,[18] this transition in Te is

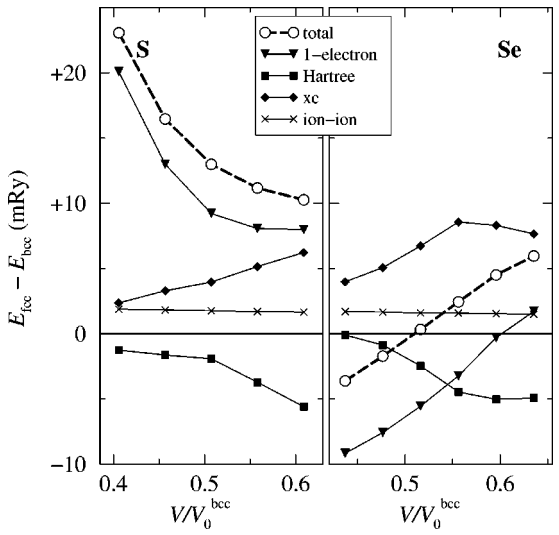

FIG. 4. Total energy difference between the fcc and bcc structures as a function of volume for S and Se. Also shown are the energy differences in the one-electron, Hartree, exchange-correlation (xc), and ion-ion contributions to the total energy. Volumes are measured with respect to the theoretical zero-pressure volumes of $V_0^{bcc}=98.6$ and 125.9 a.u./atom calculated for bcc S and Se, respectively.

found close to the experimentally measured transition pressure of 27 GPa. In addition, we find that the close-packed fcc structure becomes stable above about 80 GPa. Finally, as in Se, the sc structure is calculated to be energetically unfavorable as a high-pressure phase of Te.[18]

III. PHONON SPECTRA, ELECTRON–PHONON COUPLING, AND SUPERCONDUCTIVITY

A. Method

The density-functional linear response method[19] is used to compute the phonon spectra for each structure at several different pressures. The dynamical matrices are computed using the scheme described in Ref. 20, where the self-consistent change in the Hamiltonian caused by ionic displacements is obtained by solving a Bethe-Saltpeter equation for the change in the charge density. The dynamical matrix is computed on a grid of 6^3 phonon wave vectors $\mathbf{q}$ for β-Po S and 8^3 wave vectors for sc and bcc S. For Se, 8^3, 10^3, and 12^3 $\mathbf{q}$ points are sampled in the full β-Po, bcc, and fcc Brillouin zones, respectively.

The matrix element for scattering of an electron from state $n\mathbf{k}$ to state $n'\mathbf{k}'$ by a phonon with frequency $\omega_{\mathbf{q}\nu}$ and eigenvector $\hat{\boldsymbol{\epsilon}}_{\mathbf{q}\nu}$ is given by

$$g(n\mathbf{k},n'\mathbf{k}',\mathbf{q}\nu)=\sqrt{\frac{\hbar}{2M\omega_{\mathbf{q}\nu}}}\langle n\mathbf{k}|\hat{\boldsymbol{\epsilon}}_{\mathbf{q}\nu}\cdot\boldsymbol{\nabla}_{\mathbf{R}}V_{\mathrm{SCF}}|n'\mathbf{k}'\rangle, \tag{1}$$

where $\boldsymbol{\nabla}_{\mathbf{R}}V_{\mathrm{SCF}}$ is the gradient of the self-consistent potential with respect to atomic displacements. This scattering gives rise to a finite phonon linewidth,

$$\gamma_{\mathbf{q}\nu}=2\pi\omega_{\mathbf{q}\nu}[N(E_F)]^2\langle\langle|g_{\mathbf{q}\nu}|^2\rangle\rangle, \tag{2}$$

TABLE I. Calculated values of structural, vibrational, and electron-phonon parameters for β-Po, sc, and bcc S at various pressures. The electronic density of states at the Fermi level $N(E_F)$ is in units of states/eV/spin/cell.

	P (GPa)	V (a.u.)	α_r	$N(E_F)$	$\langle\omega\rangle$ (meV)	$\langle\omega_{\ln}\rangle$ (meV)	λ
	160	57.87	104.0°	0.148	46.4	37.7	0.76
β-Po	200	54.22	104.1°	0.143	50.6	40.2	0.76
	280	48.77	104.4°	0.140	57.2	42.3	0.61
	280	47.80	90.0°	0.159	71.8	48.1	0.52
sc	320	46.14	90.0°	0.146	76.5	52.8	0.44
	550	39.77	90.0°	0.118	91.8	57.8	0.35
bcc	550	38.81	109.5°	0.136	67.0	50.0	0.70

where $N(E_F)$ is the electronic density-of-states per spin at the Fermi level. The double brackets $\langle\langle\ldots\rangle\rangle$ denote a doubly constrained Fermi surface average as defined in Ref. 21. This scattering process also contributes to the effective mass of the electrons via the mass enhancement parameter λ, obtained from the wave-vector- and branch-dependent contributions

$$\lambda_{\mathbf{q}\nu}=\frac{\gamma_{\mathbf{q}\nu}}{\hbar\pi\ N(E_F)\omega_{\mathbf{q}\nu}^2} \tag{3}$$

by summing over branches ν and averaging over wave vectors $\mathbf{q}$.

The electron–phonon spectral function, which measures the effectiveness of phonons of a given energy to scatter electrons on the Fermi surface, plays a central role in the Eliashberg strong-coupling theory of superconductivity. The spectral function is given by

$$\alpha^2F(\omega)=\frac{1}{2\pi N(E_F)}\sum_{\mathbf{q}\nu}\ \delta(\omega-\omega_{\mathbf{q}\nu})\frac{\gamma_{\mathbf{q}\nu}}{\hbar\omega_{\mathbf{q}\nu}}. \tag{4}$$

Within this framework, the mass enhancement parameter λ is proportional to the inverse-frequency moment of the spectral function.

In the density-functional linear-response method, $\boldsymbol{\nabla}_{\mathbf{R}}V_{\mathrm{SCF}}$ is computed in the process of determining the dynamical matrices. Therefore we calculate the electron-phonon matrix elements on the same grid of wave vectors used in the phonon calculations. For calculations of the phonon density-of-states and electron-phonon spectral function, which involve summing over $\mathbf{q}$ points throughout the Brillouin zone, a Fourier interpolation procedure is used to obtain the dynamical matrix and its dissipative part on a denser mesh of $\mathbf{q}$ points.[22] The doubly constrained Fermi-surface average of g is computed using Bloch functions on dense meshes of at least 30^3 $\mathbf{k}$ and $\mathbf{k}'$ points in the full Brillouin zone, with delta functions at the Fermi level replaced by Gaussians of width of order 0.01 Ry chosen to reproduce the value of $N(E_F)$ obtained using the linear tetrahedron method.[23]

TABLE II. Calculated values of structural, vibrational, and electron-phonon parameters for β-Po, bcc, and fcc Se at various pressures. The electronic density-of-states at the Fermi level $N(E_F)$ is in units of states/eV/spin/cell.

	P (GPa)	V (a.u.)	α_r	$N(E_F)$	$\langle\omega\rangle$ (meV)	$\langle\omega_{\ln}\rangle$ (meV)	λ
	60	93.33	104.1°	0.180	23.5	18.8	0.58
β-Po	80	87.37	104.8°	0.176	25.5	19.5	0.54
	100	83.20	105.2°	0.174	27.4	21.6	0.50
	120	78.73	109.5°	0.201	26.6	17.6	0.89
	140	75.80	109.5°	0.193	28.3	18.8	0.76
bcc	160	73.32	109.5°	0.187	29.4	17.6	0.77
	220	67.36	109.5°	0.182	33.3	21.2	0.73
	260	64.25	109.5°	0.175	35.6	21.4	0.71
fcc	260	63.82	60.0°	0.183	34.93	25.23	0.59

B. Results and discussion

Tables I and II list parameters that characterize the phonon spectra and electron-phonon couplings in the high-pressure phases of S and Se. Included are the average phonon frequency $\langle\omega\rangle$ and the logarithmic λ-weighted average phonon frequency $\langle\omega_{\ln}\rangle=\exp[\Sigma_{\mathbf{q}\nu}\lambda_{\mathbf{q}\nu}\ln(\omega_{\mathbf{q}\nu})/\Sigma_{\mathbf{q}\nu}\lambda_{\mathbf{q}\nu}]$. Some of the values for $N(E_F)$ and λ listed in Table I differ by a few percent from those published in our earlier paper[11] on S because we use the more accurate tetrahedron method for calculating the electronic density-of-states in the present paper.

Within each structural phase, compression stiffens the lattice and weakens the electron-phonon interaction, as indicated by the rise in $\langle\omega\rangle$ and fall in λ. The pressure dependence of λ varies from structure to structure. In sc S, λ varies approximately as $1/\langle\omega\rangle^2$, as might be expected from Eq. (3). In β-Po S, β-Po Se, and bcc Se, however, the pressure dependence of λ is much weaker. These differences can be understood by examining contributions to λ from different phonon modes.

In some of the structural phases, it is possible to identify specific phonon modes that contribute strongly to λ. In the β-Po phase of Se, for example, there are strong anomalies in the phonon-dispersion curves along the Γ to F direction [i.e., the $(1\bar{1}0)$ direction in terms of the reciprocal lattice vectors $\mathbf{b}_i$], as shown in Fig. 5. Similar but less pronounced anomalies exist in the β-Po phase of S. These anomalies are associated with nesting of the Fermi surface by the wave vector $\mathbf{q}\approx 0.7(\mathbf{b}_1-\mathbf{b}_2)$, as confirmed by calculations of the geometric nesting factor $\langle\langle\delta(\mathbf{k}-\mathbf{k}'-\mathbf{q})\rangle\rangle$. The strong Fermi-surface nesting affects not only the phonon frequencies, but the linewidths as well. The combination of low frequencies and enhanced linewidths results in a large contribution to λ from this part of the β-Po Brillouin zone. Anomalies are also present in the phonon spectra of bcc S and bcc Se. Figure 6 shows the dispersion curves for bcc Se at 120 GPa. While not correlated with nesting vectors, the low-frequency anomalies in the transverse branches along the Γ to N and Γ to H lines nevertheless give large contributions to λ.

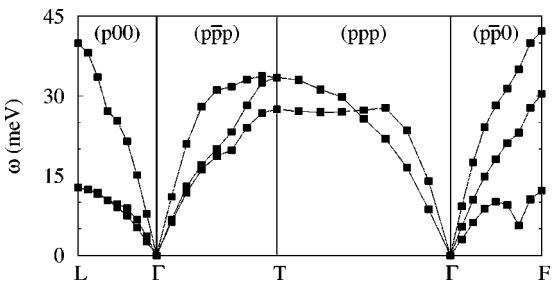

FIG. 5. Phonon-dispersion curves in β-Po Se at 60 GPa. Directions are specified in terms of reciprocal-lattice basis vectors. Soft phonon anomalies related to nesting of the Fermi surface are evident along the Γ to F line.

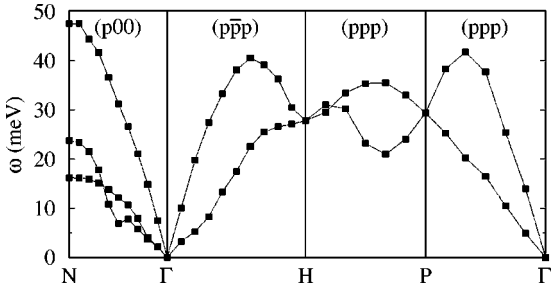

FIG. 6. Phonon-dispersion curves in bcc Se at 120 GPa. Directions and polarizations are specified in terms of reciprocal-lattice basis vectors. Phonon anomalies are present in the $(\bar{1}1)$-polarized branch along Γ to N, and in the transverse branches along Γ to H.

The soft phonon anomalies in the bcc and β-Po phases are more weakly pressure-dependent than the overall phonon spectrum. The pressure dependence of λ in these phases is strongly influenced by these persistent anomalies and is therefore weaker than the $\langle\omega\rangle^{-2}$ dependence suggested by Eq. (3). In sc S, the electron-phonon coupling is not found to be dominated by any particular phonon mode, so the pressure dependence of λ, is to a good approximation, determined by that of the average phonon frequency.

As can be seen in Tables I and II, transformations from structure to structure are usually accompanied by abrupt changes in the phonon and electron-phonon parameters. In comparing the various structural phases of S, the simple-cubic phase stands out in having the weakest electron-phonon coupling parameters. The spectral function for sc S, plotted in Fig. 7, is strikingly different from those of bcc and β-Po S. Both the average and maximum phonon frequencies in the sc phase are much larger than those in the other phases. The higher frequencies in the sc phase are due to the shorter nearest-neighbor distances and the strong concentration of charge along the bonds in the open sc lattice. With these stiff bonds, the $(1\bar{1}0)$-polarized transverse branch along the (110) direction and both of the transverse branches along the (111) direction are nearly as high in energy as the longitudinal branches. This leads to a phonon density-of-states and a spectral function that are dominated by a high-frequency peak. The large phonon energy scale and the lack of low-energy modes that couple strongly to electrons, as

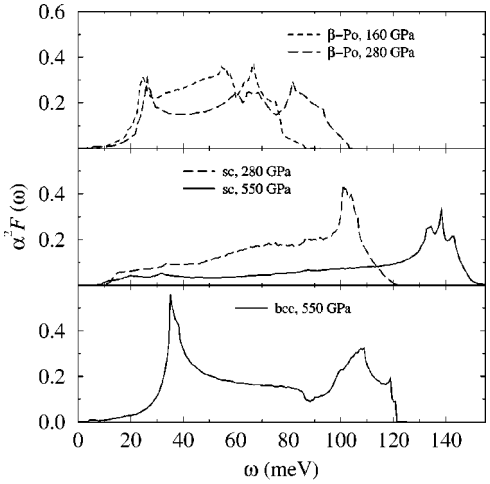

FIG. 7. Electron-phonon spectral functions calculated for β-Po, sc, and bcc S. Results for $p \leqslant 280$ GPa are reproduced from Ref. 11 to facilitate comparison over a wider range of pressures.

evidenced by the relatively large value of $\langle \omega_{\ln} \rangle$, combine to drive λ down in the sc phase of S.

Among the high-pressure phases of Se, the bcc phase stands out in that λ is largest in this phase. Although the average phonon frequencies are similar to those in the neighboring phases near the transition pressures, $\langle \omega_{\ln} \rangle$ is significantly depressed in the bcc phase. This is a sign of the importance of the low-frequency anomalies already identified in the bcc Se phonon spectra. These anomalies enhance the spectral function at low energies, as shown in Fig. 8, and they have a significant effect on λ because they appear at low frequencies. Although β-Po Se also has soft phonon anomalies, there are fewer of them due to the lower symmetry of the lattice, and they have a smaller effect on λ. No comparable soft phonon anomalies are found in the fcc phase.

In comparing analogous structural phases of S and Se, the differences in electron-phonon coupling strength reflect not only differences in the phonon spectra, but also differences in the electron-phonon matrix elements. The stronger potential in S gives rise to a larger change in the bare potential $\nabla_{\mathbf{R}} V_{\text{bare}}$ when atoms are displaced. Furthermore, because the d electrons are more tightly bound in S, these electrons are less effective in screening $\nabla_{\mathbf{R}} V_{\text{bare}}$. In combination, these two effects result in significantly larger matrix elements of $\nabla_{\mathbf{R}} V_{\text{SCF}}$ in S than in Se. Combined with the smaller mass in S, this leads to larger linewidths. This is evident in both the β-Po and bcc phases, where the phonon frequencies in S are a factor of 2 or more higher than those in Se, yet the mass enhancement parameters in the two materials are close.

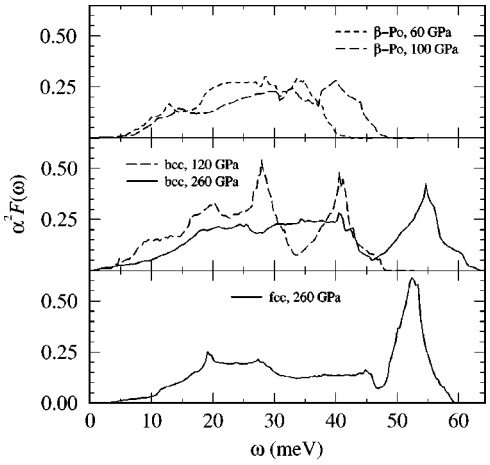

FIG. 8. Electron-phonon spectral functions calculated for β-Po, bcc, and fcc Se.

Our results can be compared to earlier density-functional-based studies of the electron-phonon interaction in β-Po and bcc Te and Se, and in bcc S.[10,24,25] Soft phonon anomalies very similar to those discussed here, have been identified to be important in the electron-phonon coupling in β-Po and bcc Te.[24] In addition, the electron-phonon mass enhancement parameter has been calculated to undergo a large jump at the β-Po to bcc transition in Te, just as we find for Se. Similar results have been reported in a recent theoretical study of the superconducting properties of bcc and β-Po Se.[25] For bcc S, our value of $\lambda = 0.70$ at 550 GPa is somewhat larger than the value of 0.58 reported in Ref. 10 for a slightly higher pressure of 584 GPa. Since values of $\lambda_{\mathbf{q}\nu}$ are in reasonable agreement along high-symmetry directions, it is likely that the difference arises from a difference in sampling of wave vectors. In the present paper, a uniform grid of points throughout the Brillouin zone is sampled, while in Ref. 10, $\lambda_{\mathbf{q}\nu}$ is calculated along a few high-symmetry directions and spherically averaged to estimate λ.

C. Making contact with experiments

The need to carry out experiments inside high-pressure cells limits the types of experimental probes available to investigate the electron-phonon interaction in the metallic phases of the chalcogens. In particular, the most common probe of α^2F in superconductors, quasiparticle tunneling,[26] is challenging because of the need to make well-characterized tunnel junctions connected to leads that enter the high-pressure cell.[27]

Measurement of superconducting properties such as the transition temperature T_C, the thermodynamic critical field H_C, the zero-temperature gap Δ_0, and the isotope effect on T_C, would be one avenue for probing the electron-phonon interaction.[28] Since superconducting properties depend not only on the electron-phonon spectral function α^2F, but also on the Coulomb pseudopotential μ^*, it is necessary to measure a combination of superconducting properties to get a handle on both the electron-electron and the electron-phonon parameters. In the weak-coupling regime, T_C, Δ_0, and H_C all essentially depend on the difference between λ and μ^*, rather than on α^2F and μ^* separately. In this case, T_C and the isotope effect on T_C, with their different α^2F and μ^* dependencies, would be the most useful combination of measurements.

Figure 9 shows our calculated superconducting transition temperatures for the high-pressure phases of S and Se for different values of μ^*, obtained by using the calculated α^2F functions as input to the Eliashberg equations. Available ex-

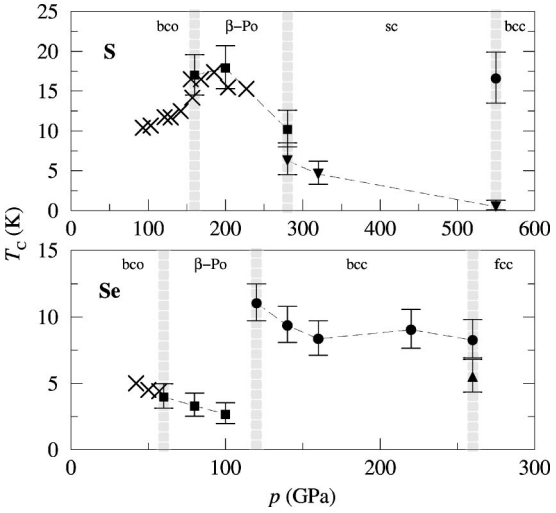

FIG. 9. Superconducting transition temperature of S and Se as a function of pressure. Squares, circles, up triangles, and down triangles represent results of calculations for the β-Po, bcc, fcc, and sc structures, respectively. The error bars show the range of T_C for $0.09<\mu^*(\omega_{\max})<0.13$ and the data points correspond to $\mu^*(\omega_{\max})=0.11$. Experimental data are plotted as crosses. The dashed lines connecting calculated points serve as guides to the eye, and the vertical gray bars roughly separate the pressure ranges over which different structures are stable.

perimental data for bco Se,[8] bco S,[9] and β-Po S,[9,29] are included. The theoretical data points in Fig. 9 correspond to $\mu^*(\omega_{\max})=0.11$, where $\omega_{\max}$ is the maximum phonon frequency. This representative value of $\mu^*(\omega_{\max})$ is chosen because it reproduces the experimentally measured T_C of 17 K at 160 GPa in S.[9] The error bars show the effect of varying $\mu^*(\omega_{\max})$ by ± 0.02. While there is no reason to assume μ^* remains constant with changes in pressure or structure, or that μ^* in Se should be the same as in S, μ^* typically lies within the range of 0.1 to 0.14 for a wide range of materials. Furthermore, a rough upper bound for μ^* given by $[\ln(E_F/\omega_{\max})]^{-1}$ suggests μ^* is less than about 0.16 in all the phases considered here.

The calculated transition temperatures follow the same trends as λ, with large increases in T_C upon transition to both bcc Se and bcc S, and downward jumps in T_C at the bcc$\rightarrow$fcc transition in Se and the β-Po$\rightarrow$sc transition in S. As reported earlier,[11] our analysis attributes the large T_C of 17 K in β-Po S, not so much to strong electron-phonon coupling, but rather to a combination of moderate coupling and a large phonon energy scale. For analogous structural phases in S and Se, the primary reason for the higher transition temperatures in S is the stiffer lattice, which sets the energy scale for T_C.

The high phonon frequencies suggest that vertex corrections might be important in these materials. The other determining factor for the strength of vertex corrections is the magnitude of the electron-phonon interaction,[30] which is moderate in both S and Se. Indeed, we estimate that the effect of the vertex corrections on T_C is on the order of 1%, and can be neglected given the uncertainty in μ^*.

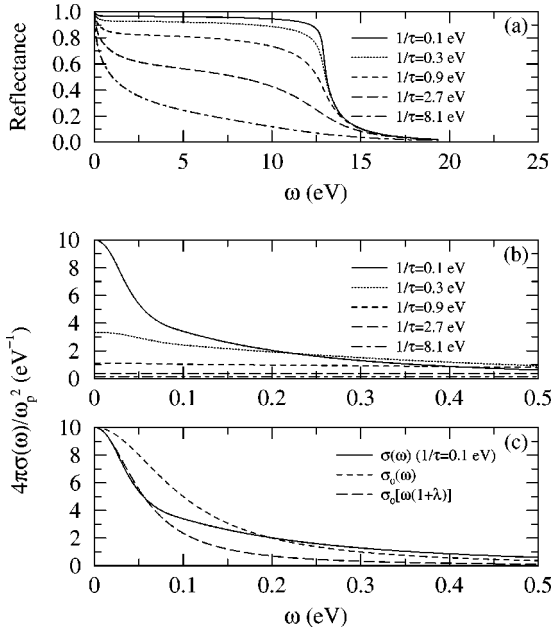

FIG. 10. Normal-state (a) reflectance and (b) optical conductivity calculated for β-Po S at 160 GPa and $T=0$ K. Results are shown for different impurity scattering times τ. In (c), the optical conductivity with $1/\tau=0.1$ eV is redrawn along with the corresponding Drude conductivity $\sigma_0(\omega)$ assuming scattering by impurities only. Also plotted is $\sigma_0[\omega(1+\lambda)]$, showing that electron-phonon scattering narrows the Drude peak by a factor of $1+\lambda$.

Although we have used the Eliashberg formalism to calculate T_C for all the phases, the coupling is sufficiently weak that the Allen-Dynes approximate formula for T_C[31] gives similar results. Furthermore, the ratios $2\Delta_0/k_BT_C$ and $\gamma T_C^2/H_C^2$, where γ is the linear coefficient of the specific heat, are calculated to be close to the BCS values of 3.53 and 1.68, respectively. For β-Po S at 160 GPa, for example, we find $2\Delta_0/k_BT_C=3.70$ and $\gamma T_C^2/H_C^2=1.66$, assuming $\mu^*(\omega_{\max})=0.11$.

As suggested above, measurement of the isotope effect on T_C would be one way to obtain more information on the Coulomb parameter. For S at 160 GPa, we estimate that the isotope exponent $\alpha=-d\ln T_C/d\ln M$ changes from 0.48 to 0.43 as μ^* is varied from 0.09 to 0.13, assuming isotopic masses M of 32 and 36. To distinguish between $\mu^*=0.09$ and $\mu^*=0.13$ then requires being able to measure T_C to an accuracy of better than 0.1 K.

Infrared spectroscopy can be used to probe α^2F independent of μ^*.[32,33] In the normal state, the phonons contribute to the optical conductivity via their renormalization of the electronic quasiparticles and by phonon-assisted scattering processes. Panels (a) and (b) in Fig. 10 show the normal-state $T=0$ reflectance and optical conductivity calculated for different values of impurity scattering rates for β-Po S at 160 GPa. The expected Holstein structure, which occurs at frequencies near the phonon frequencies, is small because the coupling strength is relatively weak. Hence, it is likely that the extraction of α^2F from phonon structure in the optical conductivity data would be challenging for this system. However, optical conductivity data could still be useful for

estimating λ. The electron-phonon interaction narrows the Drude peak associated with impurity scattering by a factor of $1+\lambda$ due to the renormalization of electronic quasiparticle energies and weights and transfers the low-frequency weight to the midinfrared region, as illustrated in Fig. 10(c). With an independent determination of the plasma frequency ω_p, the width and height of the Drude peak could be used to estimate λ.

Perhaps a simpler way to determine λ from experiments is via the dc conductivity. At temperatures on the order of the Debye temperature, the phonon-limited electrical resistivity is linear in temperature with a slope proportional to $\lambda_{tr}=2\int d\omega\, \alpha^2_{tr}F(\omega)/\omega$. Like α^2F, the transport spectral function $\alpha^2_{tr}F$ measures the effectiveness of phonons to scatter electrons on the Fermi surface, but it is weighted to take into account the change in direction of the electron velocity.[32] Experimental measurements of the electrical resistivity have been reported for the bco and lower-pressure phases of S and Se.[7,8] Extensions of these measurements to higher pressures would test our results for the electron-phonon coupling strength. Of particular interest is the linear coefficient of the resistivity in β-Po S. We calculate $\lambda_{tr}=0.78$ at 160 GPa, close to our result for λ. We believe this is the most direct way to verify our theoretical prediction that, despite the large T_C, the electron-phonon coupling is not particularly strong in this phase.

IV. CONCLUSIONS

We have presented a comparison of the pressure-induced structural phase transitions in S and Se based on density-functional calculations. Although there are some similarities in the high-pressure phase diagrams of these isovalent elements, there are also striking differences. With increasing compression, Se adopts a sequence of ever more closely packed structures (β-Po$\rightarrow$bcc$\rightarrow$fcc), while S favors more open structures (β-Po$\rightarrow$sc$\rightarrow$bcc).[11] These differences can be understood in terms of the deeper *d* pseudopotential in S arising from the lack of *d* states in the S core.

All the high-pressure phases of S and Se are calculated to have moderate electron-phonon coupling strengths and superconducting transition temperatures in the range of 0.5–20 K. Structure and pressure dependencies of the coupling strength and T_C can be understood in terms of changes in the phonon spectra. In particular, as first discussed in Ref. 11, the large observed T_C in β-Po S is calculated to arise from a combination of a moderate mass enhancement parameter λ and a large overall phonon energy scale. The large increase in λ and T_C, predicted upon transformation to the bcc phase in both S and Se, is due to the presence of soft modes in the bcc phonon spectra that strongly couple to electrons.

We suggest that measurements of the electrical resistivity as a function of temperature, the transition temperature T_C, and the isotope effect on T_C would be the most promising avenues for testing our results on the electron-phonon interaction in these compressed phases. Further, T_C measurements could be used to search for the predicted sc phase of S and the predicted fcc phase of Se since our results indicate that T_C should change abruptly when these structural transformations take place. The calculated transition pressures for both sc S and fcc Se are within the range of current diamond-anvil-cell experiments.

ACKNOWLEDGMENTS

The authors thank R. J. Hemley and V. V. Struzhkin for valuable discussions. This work was supported by the National Science Foundation under Grant No. DMR-9973225 and by the NPACI.

[1] Y. Akahama, M. Kobayashi, and H. Kawamura, Phys. Rev. B **48**, 6862 (1993).
[2] H. Luo, R.G. Greene, and A.L. Ruoff, Phys. Rev. Lett. **71**, 2943 (1993).
[3] Y. Akahama, M. Kobayashi, and H. Kawamura, Phys. Rev. B **47**, 20 (1993).
[4] K. Aoki, O. Shimomura, and S. Minomura, J. Phys. Soc. Jpn. **48**, 551 (1980).
[5] G. Parthasarathy and W.B. Holzapfel, Phys. Rev. B **37**, 8499 (1988).
[6] J. Wittig, J. Chem. Phys. **58**, 2220 (1973); K.J. Dunn and F.P. Bundy, *ibid.* **67**, 5048 (1977); F.P. Bundy and K.J. Dunn, *ibid.* **71**, 1550 (1979).
[7] F.P. Bundy and K.J. Dunn, Phys. Rev. B **22**, 3157 (1980).
[8] Y. Akahama, M. Kobayashi, and H. Kawamura, Solid State Commun. **84**, 803 (1992).
[9] V.V. Struzhkin, R.J. Hemley, H.-K. Mao, and Y.A. Timofeev, Nature (London) **390**, 382 (1997).
[10] O. Zakharov and M.L. Cohen, Phys. Rev. B **52**, 12 572 (1995).
[11] S.P. Rudin and A.Y. Liu, Phys. Rev. Lett. **83**, 3049 (1999).
[12] N. Troullier and J.L. Martins, Phys. Rev. B **43**, 8861 (1991).
[13] J. Perdew and A. Zunger, Phys. Rev. B **23**, 5048 (1981).
[14] S.G. Louie, S. Froyen, and M.L. Cohen, Phys. Rev. B **26**, 1738 (1982).
[15] H.J. Monkhort and J.D. Pack, Phys. Rev. B **13**, 5188 (1976).
[16] The bco structure, which is observed experimentally in S, Se, and Te just below the β-Po structure in pressure, is not considered in this work because we find it to be not only higher in energy than, but also mechanically unstable with respect to the β-Po structure. The instability is found in both the local-density and generalized-gradient approximations. Similar results for the bco structure are reported in Refs. 10 and 18.
[17] W. A. Harrison, *Electronic Structure and the Properties of Solids* (Freeman, San Francisco, 1980), p. 486.
[18] F. Kirchhoff, N. Binggeli, and G. Galli, Phys. Rev. B **50**, 9063 (1994).
[19] S. Baroni, P. Giannozzi, and A. Testa, Phys. Rev. Lett. **58**, 1861 (1987).
[20] A.A. Quong and B.M. Klein, Phys. Rev. B **46**, 10 734 (1992); A.Y. Liu and A.A. Quong, *ibid.* **53**, 7575 (1996).
[21] P.K. Lam, M.M. Dacorogna, and M.L. Cohen, Phys. Rev. B **34**, 5065 (1986).

[22] A.Y. Liu, Phys. Status Solidi B **217**, 419 (2000).
[23] G. Lehmann and M. Taut, Phys. Status Solidi B **54**, 469 (1972).
[24] F. Mauri, O. Zakharov, S. de Gironcoli, S.G. Louie, and M.L. Cohen, Phys. Rev. Lett. **77**, 1151 (1996).
[25] M. Otani and N. Suzuki, Phys. Rev. B **63**, 104516 (2001).
[26] E.L. Wolf, *Principles of Electronic Tunneling Spectroscopy* (Oxford University, New York, 1985).
[27] P.W. Wright and J.P. Franck, J. Low Temp. Phys. **27**, 459 (1977).
[28] J.P. Carbotte, Rev. Mod. Phys. **62**, 1027 (1990).
[29] E. Gregoryanz, V.V. Struzhkin, and R.J. Hemley (private communication).
[30] S.P. Rudin, R. Bauer, A.Y. Liu, and J.K. Freericks, Phys. Rev. B **58**, 14 511 (1998).
[31] P.B. Allen and R.C. Dynes, Phys. Rev. B **12**, 905 (1975).
[32] P.B. Allen, Phys. Rev. B **3**, 305 (1971).
[33] F. Marsiglio and J.P. Carbotte, Aust. J. Phys. **50**, 975 (1997).